A procedure for evaluating high residual stresses using the blind hole drilling method, including the effect of plasticity

M Beghini, L Bertini, and **C Santus***
Dipartimento di Ingegneria, Meccanica Nucleare e della Produzione, Universitá di Pisa, Pisa, Italy

The manuscript was received on 16 July 2009 and was accepted after revision for publication on 28 January 2010.

DOI: 10.1243/03093247JSA579

Abstract: When the blind hole drilling method is used to evaluate high residual stresses in a metallic component, plastic relaxed strain can be produced in the hole region because of the stress concentration that causes the local stresses to reach yielding. By assuming a linear–elastic behaviour of the material, a significant error can result. The present paper analyses the phenomenon of the plasticity locally induced by the introduction of the hole and proposes a procedure to take into account its effects on the residual stress evaluation. The correcting procedure has been developed by elaborating a large database of elastic–plastic finite element analyses performed considering a wide range of material properties and testing parameters, including all the strain gauge rosettes commonly used. As plasticity induces non-linearity in the relationship between residual stress and relaxed strain, the superposition principle cannot be applied, so the correction is limited to uniform in-depth residual stress fields. However, four hole depths were considered and the related correcting procedures were provided. When variable through thickness residual stress is expected, and high residual stress is confined near the surface region, the correction procedure can be applied to an initial limited depth.

Keywords: blind hole drilling method, plasticity effect, correction procedure, finite element analysis

1 INTRODUCTION

Blind hole drilling is a widely applied method for measuring residual stresses in materials that can be easily machined, such as metals. The relaxed strain field locally produced in a pre-stressed component by the introduction of the hole is generally measured by a rosette, typically carrying three strain gauges with radially oriented grids [**1**]. Recently, other methods have been proposed to measure the relaxed strain field, such as laser speckle interferometry [**2**] and Moiré interferometry [**3**]. These optical techniques provide a 'full field' detection of the relaxed displacement field near the hole, while the rosette only gives the strains in radial directions averaged on the areas of three grids. Although the optical methods can also be used to determine a non-uniform residual stress profile [**4**, **5**], the method based on the strain gauge rosette is simpler, more physically robust, and better suited to field use.

In general, residual stress evaluated by the strain gauge hole drilling method is affected by several errors or sources of inaccuracy, some of which have to be limited by improving procedural quality while others can be corrected by a proper elaboration of the results [**6**]. The present paper focuses on correcting the effect of local plasticity produced when measuring high residual stresses in ductile materials. If the level of the residual stress is comparable with the material yield stress, the stress concentration due to the hole produces zones in which the elastic limit of the material is reached. The plastic region arises at the lower circumference of the hole (the edge at the flat bottom surface), then it spreads toward the strain gauges when the hole depth is increased [**7**, **8**]. This phenomenon is significant when evaluating the most

**Corresponding author: DIMNP (Mechanical Department), University of Pisa, Largo Lucio Lazzarino, no. 2, Pisa 56122, Italy.*
email: ciro.santus@ing.unipi.it

intense and, for this reason, the most interesting residual stress fields such as those generated by shot peening [**9**, **10**], welding [**11**, **12**], or friction stir welding [**13**], particularly near the welding zone. As the plasticity makes the material more compliant, if the measured relaxed strains are elaborated by means of the usual procedures based on the assumption that the material is linear elastic, the obtained residual stress is overestimated.

The Kirsch classic solution [**14**] of the equivalent ideal two-dimensional (2D) problem represented by a plane membrane in which a passing-through hole is performed, can be used to estimate the maximum residual stress under which the material remains elastic. Note that the maximum residual stress for the elastic behaviour of the material depends on the residual stress biaxiality ratio. For instance, under uniaxial residual stress ($\sigma_x = \sigma_0$ and $\sigma_y = \tau_{xy} = 0$) the plasticity onset happens for $\sigma_0 = \sigma_Y/3$ (where σ_Y is the material yield stress), under equibiaxial residual stress ($\sigma_x = \sigma_y = \sigma_0$ and $\tau_{xy} = 0$) at $\sigma_0 = \sigma_Y/2$ and under pure shear ($\sigma_x = -\sigma_y = \sigma_0$ and $\tau_{xy} = 0$) at $\sigma_0 = \sigma_Y/4$. Even though the Kirsch solution is valid only in the plane problem, a finite element (FE) analysis shows that similar elastic limits can be assumed for a *deep* blind hole performed on a *thick* plate, under uniform through-thickness biaxial residual stress. According to the ASTM E 837-08 standard, a deep hole has to have a minimum depth of 0.4, the rosette mean diameter D, and the plate is considered thick if its thickness is at least $1.2D$ [**1**].

Nevertheless, an ideal blind hole shows a sharp notch at the lower circumference of the hole and in an elastic analysis a stress singularity is expected. Consequently, plasticity occurs at the lower circumference of the hole for any hole depth with any non-zero residual stress and, to be precise, the linearity between the strain gauge response and the residual stress is lost even for very low residual stress and any biaxiality ratio. However, accurate elastic–plastic numerical solutions demonstrate that the strain reading is affected by the plasticity only when a significant volume of the region surrounding the hole exceeds the yield limit. Moreover, considering the practical application of the testing procedure, the maximum stress that can be accurately evaluated by means of the elastic elaboration of the blind hole drilling method is even larger than that predicted by the plane Kirsch solution. Indeed, the ASTM E837-08 standard suggests that the elastic elaboration of the relaxed strain can be accepted up to a maximum residual stress of $0.6\sigma_Y$, after the cited study of Beghini *et al.* on the effect of plasticity [**15**].

However, if the residual stress measured by the ASTM E837-08 standard is higher than $0.6\sigma_Y$, the obtained value has to be considered as overestimated and the measurement rejected. In the present paper, a correction procedure by which the ASTM E837-08 standard can be extended up to σ_Y, taking into account the plasticity, is proposed. The present work is an extension and an improvement of the preliminary proposal of Beghini *et al.* [**16**, **17**]. A more accurate FE elastic–plastic parametric analysis has been developed and a more accurate, and general, correcting procedure is provided which can be applied to all the rosettes available on the market. Moreover, the previous research was limited to the deep hole configuration while, in the present study, four-hole depth configurations were investigated. This can be considered a first step in the solution of the complex and yet unsolved problem of the measurement of high and variable through thickness residual stress. Indeed, one of the main limitations of any plasticity correction procedure is due to the fact that the superimposition principle is not applicable. As a consequence, a uniform through-thickness residual stress distribution has to be assumed across the entire hole depth, as depicted in Fig. 1, and then the information gained by measuring the relaxed strains at incremental depths cannot be directly considered. In the present paper, this limitation is partially overcome by proposing a correction procedure for each of four hole depth configurations. If the residual stress is not expected to have a uniform distribution, approximate averaged residual stress levels can be deduced

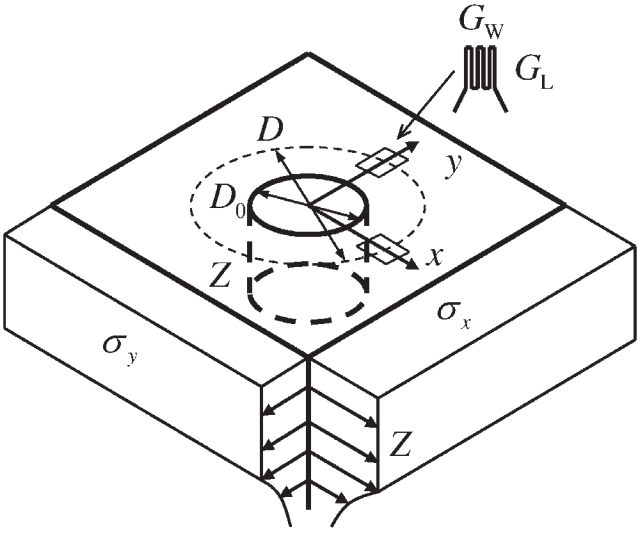

Fig. 1 Blind hole drilling scheme; principal residual stresses are assumed uniform across the hole depth (adapted from ASTM E837-08 [**1**])

at the different depths (the uniform stress is acceptable at least in the first step, which is very shallow). By comparing the different residual stresses calculated as uniform for the partial hole depths, an indication of the trend is obtained.

The method described in the paper, taking into account the hole-drilling plasticity effect, requires the advance knowledge of the principal stress directions, because the strain gauge rosette, Fig. 1, must be attached to the test specimen such that the two orthogonal grids are aligned with the principal stresses, and only the two orthogonal grids' relaxed strain readings are used. If the rosette is not aligned with the principal directions and plastic deformations are significant, the three-grid strain gauge rosette, typically used for hole-drilling measurements, do not provide sufficient information. The use of a four-grid strain gauge rosette has been suggested in reference [**17**] to evaluate the principal directions misalignment angle and reproduce the relaxed strain as principally aligned, then to be used as input for the procedure.

2 STRAIN GAUGE ROSETTES

All the rosettes available on the market for residual stress evaluation have been considered in the present analysis, see Table 1. As the grid dimensions are not very different, the corresponding calibration coefficients are quite similar. However, in this kind of measurement and elaboration, any source of errors has to be reduced as much as possible because apparently small differences can also produce non-negligible biases. The rosettes HBM RY61K and HBM RY61S have different grid layouts but the same grid dimensions – D, G_L, G_W – so they have the same response to plasticity. The Vishay 062RE type is actually a group of three similar rosettes with gauge circle diameters: $D = 2.57$, 5.13, 10.26 mm and proportional grid length and width G_L, G_W. Also, the plasticity effect is the same because of the similarity of the geometry.

The ASTM E837-08 standard indicates type A rosettes with the grids spaced according to the 0°/90°/135° pattern, while type B has grids at 0°/45°/90°. The angular difference is important when the principal direction of the residual stress field has to be obtained and when the eccentricity is considered [**20**]. In the present study, the different sequence of grid angles does not play any role. However, the distinction between type A and type B is relevant due to the different width of the grid.

The calibration coefficients a and b are defined in the ASTM E837-08 standard [**1**] for a uniform through-thickness residual stress up to the maximum hole depth, and assuming the material linear is elastic. Indicating by x, y the principal directions of the residual stress field and assuming that two grids are oriented in those directions, see Fig. 1, the principal residual stresses σ_x, σ_y and the measured relaxed strain ε_x, ε_y have the following relationships

$$\sigma_x = -\frac{E(\varepsilon_x+\varepsilon_y)}{2a(1+\nu)} - \frac{E(\varepsilon_x-\varepsilon_y)}{2b},$$
$$\sigma_y = -\frac{E(\varepsilon_x+\varepsilon_y)}{2a(1+\nu)} + \frac{E(\varepsilon_x-\varepsilon_y)}{2b} \quad (1)$$

where E, ν are the material Young's modulus and Poisson's ratio respectively. The calibration coefficients a and b depend on geometric quantities and the material elastic properties, and they can be obtained with a calibration procedure based on a direct measurement of a known stress field or, more conveniently, through a FE simulation of residual stress measurement. By applying a known residual stress field with $\sigma_x \neq \sigma_y$, after measuring or numerically evaluating the relaxed strain ε_x, ε_y produced by drilling the hole, equation (1) can be used to deduce the calibration coefficients a and b. The calibration coefficients are reported in Appendix 2, see Table 3, for $\nu = 0.3$ for all the considered rosettes and the several ratios: Z/D, D_0/D where Z is the hole depth and D_0 is the hole diameter. The accurate FE model used to find the calibration coefficients is explained in the following section. This model was used to perform the elastic–plastic analyses too, by introducing the specific elastic–plastic constitutive material model.

Table 1 Strain gauge rosettes and grid dimensions

Name used in the paper	Datasheet name	D (mm)	G_L (mm)	G_W (mm)	Reference
ASTM A	Vishay 062RE	5.13	1.59	1.59	[**1**, **18**]
ASTM B	Vishay 062UM	5.13	1.59	1.14	[**1**, **18**]
HBM 1	HBM RY21	10.2	3.0	2.5	[**19**]
HBM 2	HBM RY61K(S)	5.10	1.50	0.70	[**19**]
HBM 3	HBM RY61R	5.10	1.50	0.72	[**19**]

3 FE MODEL

3.1 General features

A FE model was set up numerically to evaluate the relaxed strain readings for different geometric configurations and material properties. The assumptions of the analysis and the model features are summarized below.

1. Owing to symmetries, the FE model was reduced to a quarter of the entire volume; see Fig. 2.
2. The model width was chosen 30 times the hole diameter D_0 and the thickness 1.2 times the rosette mean diameter D, according to the minimum thickness recommended by the ASTM E837-08 standard for thick plates; see Fig. 2.
3. A bilinear stress–strain curve and isotropic strain hardening plasticity model were assumed; thus material is completely defined by the elastic properties E, ν, the yield stress σ_Y, and the strain-hardening ratio $R = E_T/E$; see Fig. 3.

3.2 FE model validation

The distributions of the elements on the plane and along the depth were preliminarily examined in order to obtain an accurate numerical reproduction of the phenomenon. In this phase a linear elastic material was considered for reference. A plane stress FE model with the same element distribution was assessed by comparison with the Kirsch plane stress solution (provided by Schajer [**21**]), see Fig. 4.

The relaxed strains obtained by the plane model showed differences $e_v < 1$ per cent as compared to the analytical solution, so the in-plane element distribution was considered accurate enough.

A similar assessment of the through-thickness nodal distributions was not possible as an equivalent analytical reference solution was not available for the blind hole, even in the elastic regime. For this reason, a very refined model made by plane *harmonic* elements was set up to produce accurate reference solutions in the elastic regime. Again, the relative differences with the three-dimensional (3D)

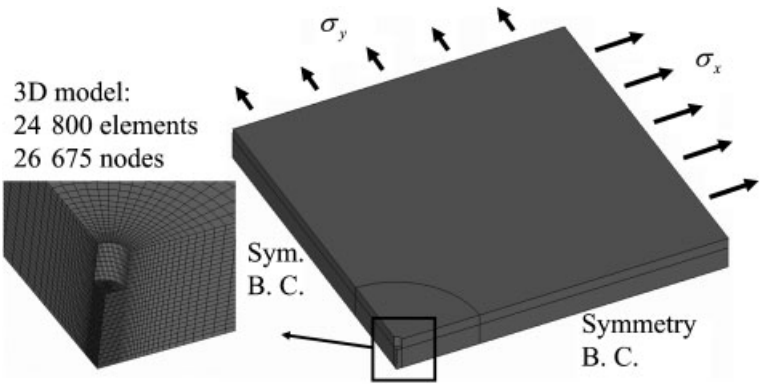

Fig. 2 Solid tridimensional FE model

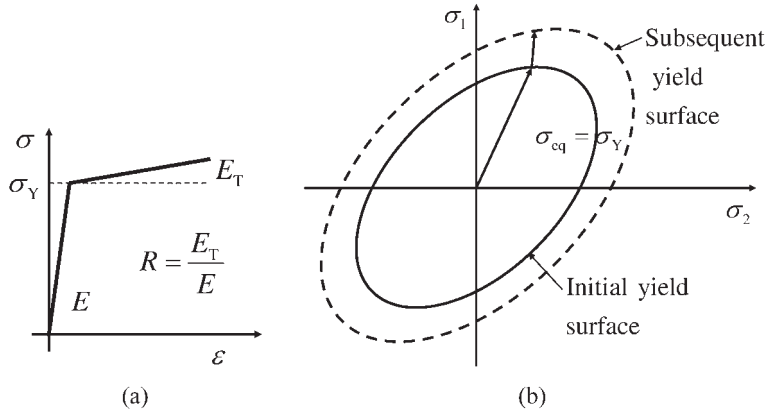

Fig. 3 Assumed material constitutive law: bilinear isotropic hardening

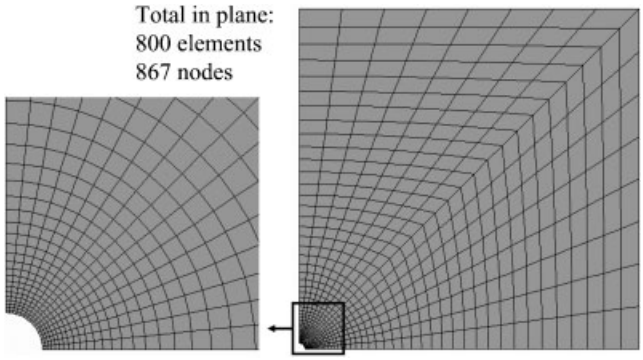

Fig. 4 Surface element distribution producing a percentage error below 1 per cent

model was below 1 per cent. Therefore, the discretization along the depth of the 3D model was also assumed to be accurate enough. The validated 3D FE model, used for all the elastic–plastic analyses reported in the following, is shown in Fig. 2.

3.3 Loading sequence

If the FE analysis is intended to reproduce accurately the plasticity generated during the hole drilling, the actual evolution of the hole on a body affected by the residual stresses should be modelled. This can be properly obtained either by using the 'birth and death' elements or by drastically reducing the Young's modulus of the elements at the layers to be removed. These two equivalent procedures are here called the 'hole-after-residual stress' approach. If the material were linear elastic, or hyperelastic at least, the relaxed strain measured by the rosette could be alternatively obtained by the 'loading-after-hole' approach, i.e. by simulating the application of the stress on a plate already carrying the hole, since the solution is not path-dependent (provided that the strain at the gauge location calculated with no hole is subtracted).

The loading-after-hole approach is the typical FE procedure used for determining the elastic calibration coefficients as it is simpler to be applied and computationally more efficient. Unfortunately, in the presence of plasticity, the final stress–strain distribution depends on the loading sequence (path-dependent solution) and the hole-after-residual stress approach should be applied. However, when plasticity occurs, the loading-after-hole approach is even more computationally efficient than the hole-after-residual stress approach, as a single load step is imposed in the former case, while multiple load steps are to be applied in the latter case. For this reason, a case study was performed and a comparison between the predictions of the two approaches was obtained for the elastic–plastic phenomenon under consideration. The results of an ASTM A rosette and typical hole diameter $D_0/D = 0.4$ are presented by comparing the loading-after-hole FE model and the hole-after-residual stress approaches applied to the same FE model under the same stress. Similar results were found for other rosettes and test parameters.

In general, the two approaches were found to produce negligible differences in terms of the relaxed strain. The relative differences were found in the order of a few per cent, even in the worst condition of an almost perfectly plastic material, and dependent on the biaxiality ratio: $\Omega = \sigma_x/\sigma_y$. The maximum difference d_p was found for $\Omega = 0.668$; see Fig. 5.

The maps of the first principal plastic strain ε_1^{pl}, obtained by following the two approaches, for the worst condition $\Omega = 0.668$, are shown in Fig. 6.

When taking the loading-after-hole approach, the region that experiences plasticity is slightly larger; however, the error due to the path dependence d_p is very small because the strain gauge grids that measure the relaxed strain are at a certain distance from the plastic region. The condition shown in the figure refers to a rather high plastic effect and the path dependence reduces quickly for a lower residual stress.

The present results do not confirm the data published in the paper by Moharami and Sattari-Far [**12**] who indicated a strong path dependence at the same loading conditions as reported here. However, in the authors' opinion, the present results appear more justifiable. Indeed, the plastic zone which can be produced in the hole drilling is dominated by the prevailing surrounding elastic

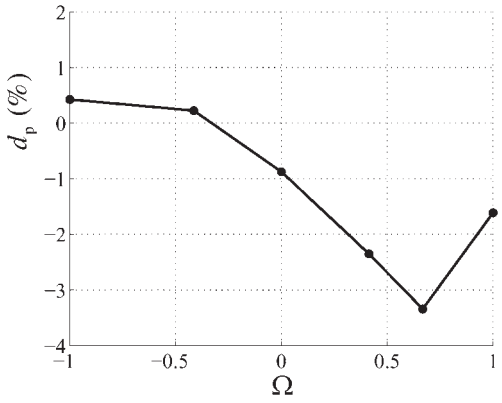

Fig. 5 Loading-after-hole to hole-after-residual stress approaches path dependency relative difference

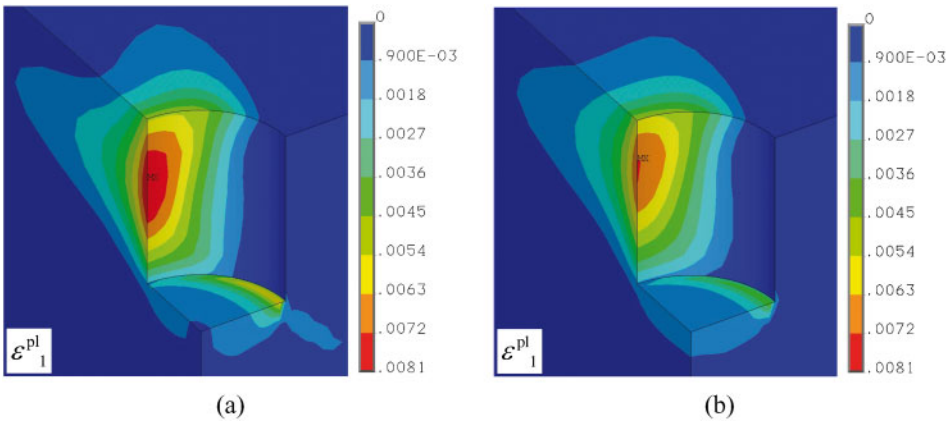

Fig. 6 First principal plastic strain, $\Omega = 0.668$, imposed residual stress very near the material yield stress: (a) the loading-after-hole approach; (b) the hole-after-residual stress approach

region and it can be verified that most points of the model experience an increasing stress history even when the hole-after-residual stress approach is applied. It is worth noting that the negligible effect of the loading sequence also gives the possibility to design experimental verifications of the elastic–plastic analysis by controlling the remote load on a specimen. The same tests would be much more difficult to obtain using several specimens affected by different and controlled residual stresses [**12**].

After having verified a general negligible effect due to the load sequence, the FE database developed in order to elaborate the correction procedure was obtained following the more efficient loading-after-hole approach: the simulation time following this approach was approximately 5 min on a modern PC desktop while with the other approach, the simulation time was 10 times higher.

3.4 Plasticity factor

The von Mises equivalent stresses $\sigma_{eq} = \sqrt{\sigma_x^2 + \sigma_y^2 - \sigma_x\sigma_y}$ was assumed to quantify the effect of biaxiality and, in accordance with reference [**17**], a dimensionless plasticity factor was introduced

$$f = \frac{\sigma_{eq} - \sigma_{eq,i}}{\sigma_Y - \sigma_{eq,i}} \tag{2}$$

where $\sigma_{eq,i}$ is the equivalent residual stress producing the onset of plasticity in the 2D case, and σ_Y is the material yield stress. The plasticity factor measures the residual stress intensity with respect to the approximate onset of plasticity given by the plane Kirsch solution. The equivalent residual stress at the plasticity onset can be expressed as a function of the biaxiality ratio $\Omega = \sigma_y/\sigma_x$, according to the plane stress Kirsch solution

$$\sigma_{eq,i} = \sigma_Y \frac{\sqrt{1 - \Omega + \Omega^2}}{3 - \Omega} \tag{3}$$

Following equations (2) and (3), $f = 0$ represents the condition of the highest residual stress that still does not produce plasticity, while $f = 1$ is related to the residual stress producing general yielding in the whole body. As previously observed, neither does a small positive plasticity factor (e.g. $f = 0.01$) produce a significant plasticity effect on the measurement, because the $\sigma_{eq,i}$ is defined according to the Kirsch plane stress model and the limited plastic region at the lower circumference of the hole, which is produced also for $f < 0$, does not significantly affect the relaxed strain on the surface as compared to the elastic field.

3.5 Investigated configurations

Any measurement configuration is defined by: rosette type, i.e. the dimensionless ratios G_L/D, G_W/D, hole diameter D_0/D and depth Z/D, biaxiality ratio $\Omega = \sigma_x/\sigma_y$, and a material strain hardening ratio $R = E_T/E$. For any configuration the readings of the rosette were obtained as a function of the residual stress level f. A database of FE simulations was produced by performing an extensive parametric analysis which is summarized in the following:

(a) rosette types with the dimensions reported in Table 1;
(b) hole diameter $D_0/D = 0.3, 0.35, 0.4, 0.45, 0.5$;
(c) strain hardening ratios $R = 0.01, 0.1, 0.25$;

(d) biaxiality ratios $\Omega = -1.000$, -0.414, 0.000, 0.414, 0.668, 1.000;
(e) plasticity factors $f = 0.0$, 0.1, 0.2, 0.3, 0.4, 0.5, 0.6, 0.7, 0.8, 0.9, 0.99;
(f) hole depths $Z/D = 0.02$, 0.1, 0.2, 0.4.

The combinations of plasticity factors and biaxiality ratios are shown in Fig. 7.

In order to take advantage of the symmetry of material properties, the condition $|\sigma_x| > |\sigma_y|$ was assumed, thus limiting the region of the Haigh-Westergaard plane $\sigma_x - \sigma_y$ to the portion reported in Fig. 7 ($|\Omega| \leqslant 1$) without reducing the generality of the results. This implies that the direction of the maximum absolute value of the measured relaxed strain has to be the x axis.

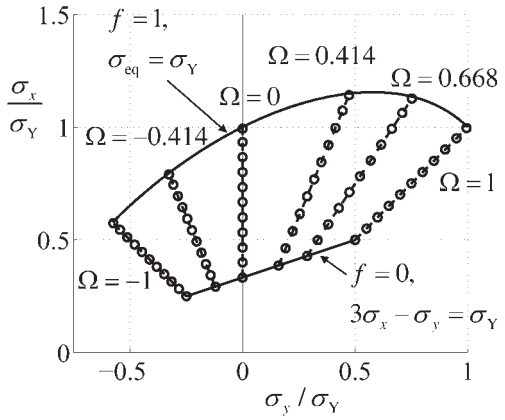

Fig. 7 Combinations of plasticity factors and biaxiality ratios

The total number of 3D elastic–plastic analyses was: $5 \times 5 \times 3 \times 6 \times 11 \times 4 = 19\,800$. A powered PC desktop takes approximately 5 min for each simulation at 100 per cent elaboration time, so approximately 1700 h (= 70 full days) were required to complete the database.

3.6 Results

Typical results of the shallow-hole and the deep-hole configurations for $\Omega = 1$, rosette-type ASTM A, diameters ratio $D_0/D = 0.4$, strain hardening ratio $R = 0.01$ are reported in Fig. 8.

It can be observed that for the shallow hole, the plastic region is located below the hole bottom surface. The plastic region reaches the surface for the deep hole, and for values of f approaching unity, particularly for materials with low strain hardening, the surface plastic boundary intersects the grid region.

After imposing the loading conditions and having obtained the solution, the simulated strain of the rosettes ε_x, ε_y were calculated from the displacement differences, along the grid direction, at the two ends of the grid divided by the grid length. The FE simulated strain was then processed by means of the elastic calibration coefficients a and b, Table 3, in order to obtain the 'as elastically evaluated' residual stresses, i.e. the stress components that would result from the measured strain by assuming that the material is linear elastic [**17**]

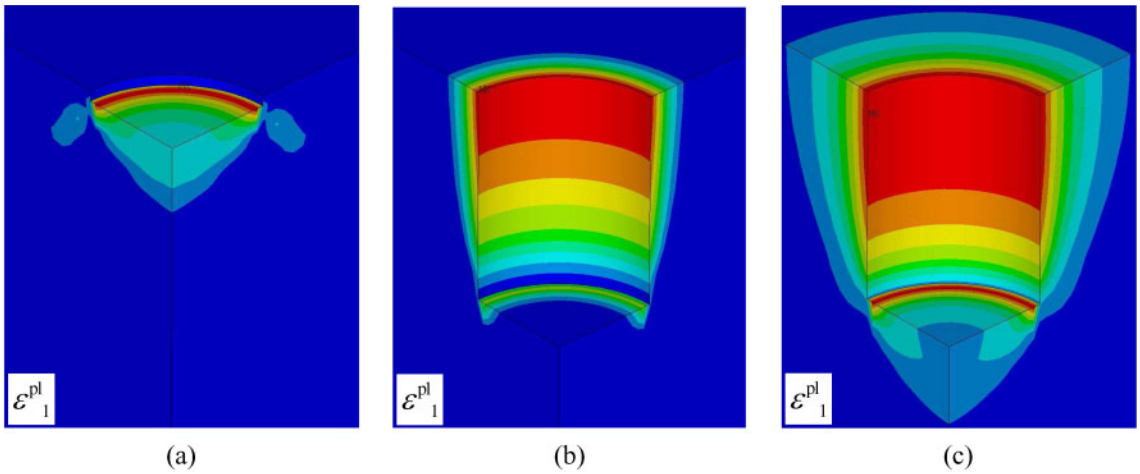

Fig. 8 First principal plastic strain distribution: (a) shallow hole, plasticity factor $f = 0.99$, maximum first principal plastic deformation $\varepsilon_1^{pl} = 0.623 \times 10^{-3}$; (b) deep hole, plasticity factor $f = 0.5$, maximum $\varepsilon_1^{pl} = 1.26 \times 10^{-3}$; (c) deep hole, plasticity factor $f = 0.99$, maximum $\varepsilon_1^{pl} = 3.20 \times 10^{-3}$

$$\sigma_{x,\mathrm{el}} = -\frac{E(\varepsilon_x - \varepsilon_y)}{2a(1+\nu)} - \frac{E(\varepsilon_x - \varepsilon_y)}{2b},$$
$$\sigma_{y,\mathrm{el}} = -\frac{E(\varepsilon_x + \varepsilon_y)}{2a(1+\nu)} + \frac{E(\varepsilon_x - \varepsilon_y)}{2b} \quad (4)$$

The elastically evaluated equivalent stress can be defined as

$$\sigma_{\mathrm{eq,el}} = \sqrt{\sigma_{x,\mathrm{el}}^2 + \sigma_{y,\mathrm{el}}^2 - \sigma_{x,\mathrm{el}}\sigma_{y,\mathrm{el}}} \quad (5)$$

and the related elastically evaluated plasticity factor is obtained by the equation

$$f_{\mathrm{el}} = \frac{\sigma_{\mathrm{eq,el}} - \sigma_{\mathrm{eq,i}}}{\sigma_{\mathrm{Y}} - \sigma_{\mathrm{eq,i}}} \quad (6)$$

So far, the ASTM interpretation procedure has been applied ignoring the effect of plasticity. Consequently, if a significant plasticity is produced, the elastically calculated plasticity factor is larger than the actual plasticity factor. As the plasticity is not expected to play a significant role for a plasticity factor near 0, it follows that $f_{\mathrm{el}} \approx f$, when $f \ll 1$. The following function

$$f_{\mathrm{el}} = f + W f^{\mu} \quad (7)$$

was found accurately to fit the relationship between f and f_{el} for any considered configuration. The expression is a novelty, compared to the proposal in reference [**17**] in which a simpler quadratic function was used. The main reason for adopting this more general expression (equation (7) becomes a quadratic expression when $\mu = 2$) is mainly due to the broader range of configurations considered in the present analysis; in particular, the shallow hole required an exponent μ significantly higher than 2. It can be observed that the asymptotic behaviour of the function at low f values is fulfilled by the proposed expression for any values of the parameters W and μ. The parameters W and μ were found for any analysed material and geometrical configuration by means of a least-square fitting, which was found to produce excellent results. Comparisons between the FE solutions and the obtained fitting curves are shown in Fig. 9 for the rosette-type ASTM A, depth $D_0/D = 0.4$ and considering the most challenging conditions for the strain hardening ratio $R = 0.01$.

In general, the obtained parameters W, μ depend on Z/D, D_0/D, Ω, R and on the rosette geometry G_{L}/D, G_{W}/D. As a unique function representing W, μ was

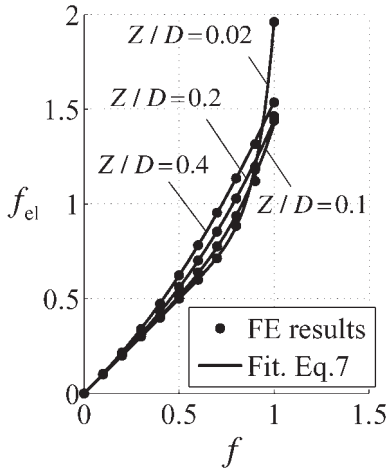

Fig. 9 Relation between the imposed plasticity factor f and the elastically calculated plasticity factor f_{el}, $R = 0.01$, $D_0/D = 0.4$, depth ratios: $Z/D = 0.02$, 0.1, 0.2, 0.4, rosette-type ASTM A

considered too complicated to be obtained with the required level of accuracy, it was decided to obtain specific functions W, μ of $\delta = D_0/D$ and Ω only for any rosette. Figure 10 shows the $W(\delta, \Omega)$, $\mu(\delta, \Omega)$ functions for the ASTM A rosette type, depth ratio $Z/D = 0.4$, and different strain-hardening ratios. Other configurations showed similar trends.

Bivariate polynomials were introduced for expressing the parameters W, m as functions of the dimensionless ratios δ and Ω. It is worth noting that both coefficient functions show a parabolic trend with respect to δ (no inversion of curvature) while they show an inversion of curvature with respect to Ω, that can be approximated with a cubic relationship. Therefore, the polynomial functions to be introduced need to have the terms in δ^2, δ, the terms in Ω^3, Ω^2, Ω, the combined terms, and the degree zero term

$$\begin{aligned} W = {} & w_1\Omega^3\delta^2 + w_2\Omega^2\delta^2 + w_3\Omega\delta^2 + w_4\delta^2 + w_5\Omega^3\delta \\ & + w_6\Omega^2\delta + w_7\Omega\delta + w_8\delta + w_9\Omega^3 + w_{10}\Omega^2 \\ & + w_{11}\Omega + w_{12} \\ \mu = {} & m_1\Omega^3\delta^2 + m_2\Omega^2\delta^2 + m_3\Omega\delta^2 + m_4\delta^2 + m_5\Omega^3\delta \\ & + m_6\Omega^2\delta + m_7\Omega\delta + m_8\delta + m_9\Omega^3 + m_{10}\Omega^2 \\ & + m_{11}\Omega + m_{12} \end{aligned} \quad (8)$$

A further least-squares fitting was then performed to find the coefficients w_i, $m_i (i = 1, \ldots, 12)$. The final results are reported in Table 4 of Appendix 2 for all

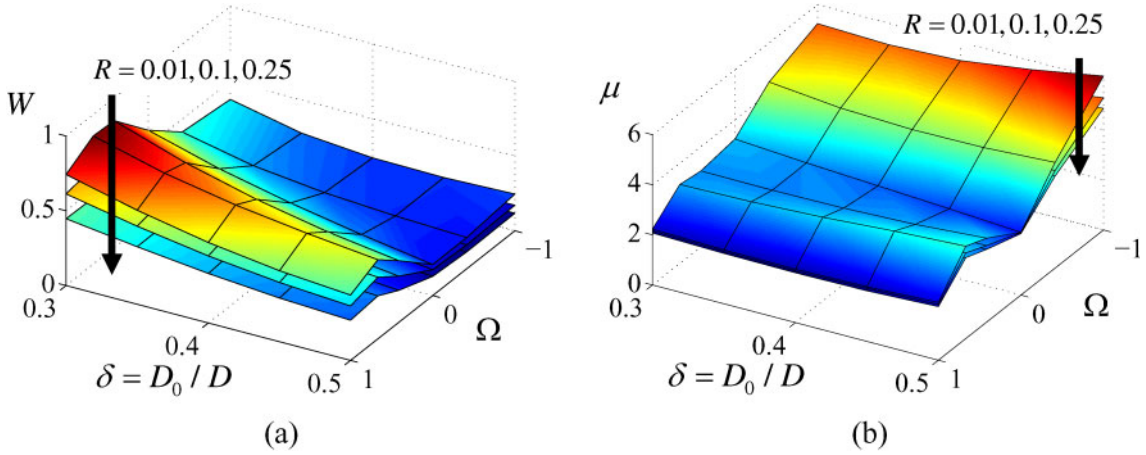

Fig. 10 Rosette-type ASTM A, $Z/D = 0.4$, different strain hardening ratios $R = 0.01$, 0.1, 0.25: (a) $W(\delta, \Omega)$, (b) $m(\delta, \Omega)$

the rosettes, strain-hardening ratios, and hole depths.

3.7 Effect of stress biaxiality

The present FE simulations confirmed the observation that the ratio between the measured relaxed strains along the principal directions $\varepsilon_x/\varepsilon_y$ depends on the stress ratio Ω but it is almost unaffected by the plasticity factor, as shown in Fig. 11. As a consequence, the biaxiality ratio Ω can be approximated by the ratio between the elastically calculated residual stress components $\sigma_{x,\mathrm{el}}$, $\sigma_{y,\mathrm{el}}$

$$\Omega = \frac{\sigma_y}{\sigma_x} \approx \Omega_{\mathrm{el}} = \frac{\sigma_{y,\mathrm{el}}}{\sigma_{x,\mathrm{el}}} \tag{9}$$

As explained in the following, this approximate relationship is particularly useful for simplifying the correction procedure.

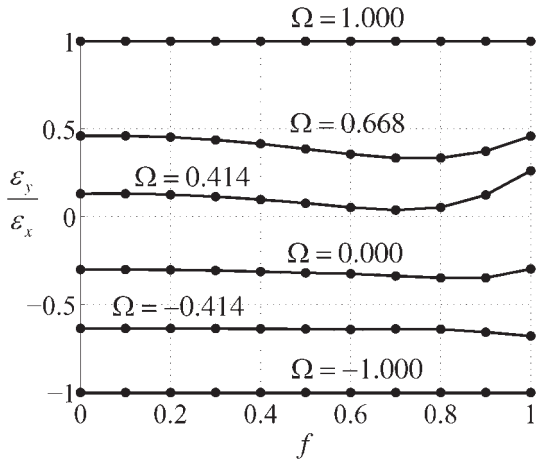

Fig. 11 Weak dependence of the ratio between the relaxed strain on the plasticity factor

4 CORRECTION PROCEDURE FOR THE EFFECT OF PLASTICITY

The elaboration of the FE results explained in the previous sections gives the tools for developing a procedure to measure high residual stress which includes a correction of the elastically evaluated stress in order to account for the plasticity effect, if necessary. The procedure is summarized in the following steps.

1. The strain gauge rosette is applied to the surface of the body affected by residual stress with the 1 and 3 grids aligned with the known (or at least assumed) principal residual stress directions and the signals are set to 0.
2. The relaxed strains ε_1, ε_2, ε_3 are measured after the hole, the x axis is chosen parallel to the grid measuring the maximum absolute value; therefore, if $|\varepsilon_1| > |\varepsilon_3|$, then $\varepsilon_x = \varepsilon_1$ and $\varepsilon_y = \varepsilon_3$, otherwise $\varepsilon_x = \varepsilon_3$ and $\varepsilon_y = \varepsilon_1$.
3. The elastically evaluated residual stresses $\sigma_{x,\mathrm{el}}$, $\sigma_{y,\mathrm{el}}$ are determined from equation (4).
4. The elastically calculated biaxiality ratio Ω_{el} is assumed to be an accurate approximation of the actual residual stress biaxiality ratio Ω, equation (9).
5. f_{el} can be obtained from equation (6), with the equivalent residual stress at the yield onset $\sigma_{\mathrm{eq,i}}$ obtained from equation (3).
6. If $f_{\mathrm{el}} < 0$, no correction is required and the elastically evaluated residual stresses are assumed as the actual residual stresses; otherwise, the

plastic correction is required and the procedure continues in the following steps:

(a) the coefficients w_i, $m_i (i = 1 \ldots 12)$ are obtained from Table 4 for the given rosette hole depth and material;
(b) the coefficients W, μ are obtained from equation (8);
(c) the actual f has to be obtained from f_{el} by inverting equation (7); to solve this unelementary equation, the Newton–Raphson algorithm is recommended which gives an accurate numerical approximation of the plasticity factor, hereafter called $\hat{f}$; for details, see Appendix 3;
(d) the estimated equivalent residual stress $\hat{\sigma}_{eq}$ is obtained from the plasticity factor $\hat{f}$

$$\sigma_{eq} = \sigma_{eq,i} + \hat{f}\left(\sigma_Y - \sigma_{eq,i}\right) \tag{10}$$

(e) Finally, the estimated principal residual stress components $\hat{\sigma}_x$, $\hat{\sigma}_y$ are obtained from $\hat{\sigma}_{eq}$

$$\hat{\sigma}_x = \hat{\sigma}_{eq} \frac{1}{\sqrt{1 - \Omega + \Omega^2}}, \quad \hat{\sigma}_y = \Omega \hat{\sigma}_x \tag{11}$$

A numerical example of the practical application of the procedure is reported hereafter. As shown in Fig. 12, the measurement of a through-thickness uniform uniaxial tensile residual stress was numerically simulated with the following parameters: material yield stress $\sigma_Y = 500$ MPa, strain-hardening ratio $R = 0.01$, $\sigma_x = 0.95\sigma_Y = 475$ MPa (not equivalent to $f = 0.95$), ASTM A rosette with diameter $D = 5.13$ mm, and hole $D_0 = 0.4D$.

All the quantities obtained during the application of the procedure are reported in Table 2 for the four hole depths $Z_1 = 0.02D$, $Z_2 = 0.1D$, $Z_3 = 0.2D$, and $Z_4 = 0.4D$.

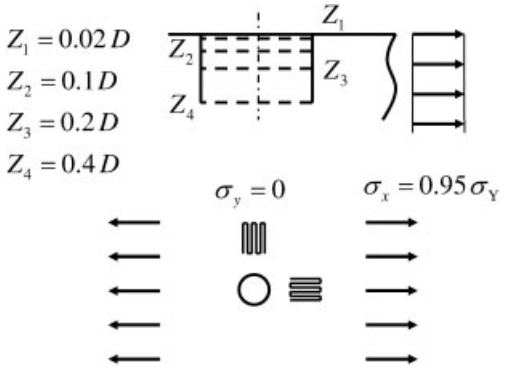

Fig. 12 Monoaxial high residual stress to be reproduced by the blind hole drilling method and the plasticity effect correction

Table 2 also shows the relative error (per cent) between the estimated residual stress assuming the material as elastic $\sigma_{eq,el}$, i.e. not taking into account the plasticity effect, and the (actual) equivalent stress σ_{eq}. It is worth noting that this error is in the range 15–18 per cent, while the error of the correction procedure itself $(\hat{\sigma}_x - \sigma_x)/\sigma_x$ is much lower (3–5 per cent).

5 DISCUSSION

Because of the introduced approximations (mainly due to the fitting functions and the assumed independence of the biaxiality ratio to the stress level) the procedure is not expected to reproduce exactly the imposed value, even in a calibration experiment made by a numerical simulation. The 'self consistency' of the model was therefore tested in order to estimate the capability of the procedure to reproduce residual stress imposed in a condition in which the other errors are not present. The numerically evaluated relaxed strains were then elaborated by the proposed correcting procedure

Table 2 Values obtained in the application examples ($1\,\mu\varepsilon = 10^{-6}$ mm/mm)

$Z_1 = 0.02D$	$Z_2 = 0.1D$	$Z_3 = 0.2D$	$Z_4 = 0.4D$
$\varepsilon_x = -65.4\,\mu\varepsilon$	$\varepsilon_x = -451.4\,\mu\varepsilon$	$\varepsilon_x = -774.4\,\mu\varepsilon$	$\varepsilon_x = -945.0\,\mu\varepsilon$
$\varepsilon_y = 12.8\,\mu\varepsilon$	$\varepsilon_y = 123.3\,\mu\varepsilon$	$\varepsilon_y = 229.9\,\mu\varepsilon$	$\varepsilon_y = 327.1\,\mu\varepsilon$
$\sigma_{x,el} = 553$ MPa	$\sigma_{x,el} = 552$ MPa	$\sigma_{x,el} = 537$ MPa	$\sigma_{x,el} = 552$ MPa
$\sigma_{y,el} = -20$ MPa	$\sigma_{y,el} = -56$ MPa	$\sigma_{y,el} = -41$ MPa	$\sigma_{y,el} = -29$ MPa
$f_{el} = 1.190$	$f_{el} = 1.248$	$f_{el} = 1.179$	$f_{el} = 1.202$
$\Omega_{el} = -0.036$	$\Omega_{el} = -0.102$	$\Omega_{el} = -0.077$	$\Omega_{el} = -0.052$
$\sigma_{eq,i} = 168$ MPa	$\sigma_{eq,i} = 170$ MPa	$\sigma_{eq,i} = 169$ MPa	$\sigma_{eq,i} = 168$ MPa
$W = 1.218$, $\mu = 16.0$	$W = 0.504$, $\mu = 6.36$	$W = 0.340$, $\mu = 4.47$	$W = 0.380$, $\mu = 3.34$
$\hat{f} = 0.912$	$\hat{f} = 0.930$	$\hat{f} = 0.932$	$\hat{f} = 0.917$
$\hat{\sigma}_x = 462$ MPa	$\hat{\sigma}_x = 452$ MPa	$\hat{\sigma}_x = 459$ MPa	$\hat{\sigma}_x = 460$ MPa
$\hat{\sigma}_y = -17$ MPa	$\hat{\sigma}_y = -46$ MPa	$\hat{\sigma}_y = -35$ MPa	$\hat{\sigma}_y = -24$ MPa
$(\hat{\sigma}_x - \sigma_x)/\sigma_x = -2.7\%$	$(\hat{\sigma}_x - \sigma_x)/\sigma_x = -4.8\%$	$(\hat{\sigma}_x - \sigma_x)/\sigma_x = -3.4\%$	$(\hat{\sigma}_x - \sigma_x)/\sigma_x = -3.1\%$
$(\sigma_{eq,el} - \sigma_{eq})/\sigma_{eq} = 16\%$	$(\sigma_{eq,el} - \sigma_{eq})/\sigma_{eq} = 18\%$	$(\sigma_{eq,el} - \sigma_{eq})/\sigma_{eq} = 15\%$	$(\sigma_{eq,el} - \sigma_{eq})/\sigma_{eq} = 17\%$

and the obtained residual stresses compared to the applied values, Fig. 13. It can be observed that the maximum error was ± 4 per cent at the highest residual stress level ($f = 0.99$) and low strain-hardening coefficients ($R = 0.01$), while the relative difference is typically within ± 1–2 per cent.

It is worth noting that during the real application of the procedure, several significant measurement issues are important, such as: hole eccentricity, hole diameter uncertainty, and material properties not accurately known, in particular, the yield stress and the strain hardening near the yielding point. It is also worth noting that some of these important sources of error affect the residual stress evaluation in the elastic regime as well. Consequently, the estimated plasticity factor $\hat{f}$ can differ from the actual plasticity factor f, not only for numerical approximations but, more probably, for these other sources of error. Considering this fact, the errors introduced by the inexact self-consistency of the proposed correcting procedure can be considered to be negligible.

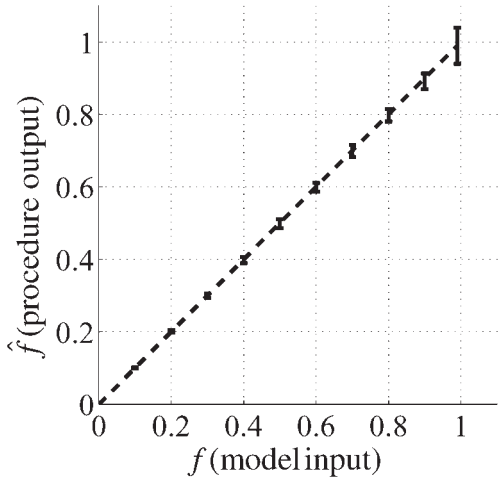

Fig. 13 Model self-consistency for all 14 850 analysed configurations

A limitation of the procedure is that the residual stress has to be uniform over the entire hole depth, so variable through-thickness residual stress cannot be completely deduced. The plasticity correction procedure is recommended if the residual stress is near the material yield stress, especially when elaborating a shallow hole, otherwise f and f_{el} are close and the correction is small. As a general indication, considering the model self-consistency and the need to assume uniform stress, the use of the correcting procedure is effective when the correction is higher than 3–5 per cent of the material yield stress. In Fig. 14(a), the equibiaxial stress state $\Omega = 1$ shows that the difference between the elastically evaluated equivalent residual stress and the actual equivalent residual stress is larger than 5 per cent of the yield stress when the residual stress is higher than 70 per cent of the yield stress for the deep-hole configuration, and higher than 80–90 per cent of the yield stress for the shallower hole configurations. These boundaries are even higher for a lower biaxiality stress ratio; Fig. 14(b). This important effectiveness boundary (and its dependencies with the depth and stress biaxiality ratio) can be considered an update of the conservative 60 per cent that is reported, at present, in the ASTM E837-08 standard [**1**].

The proposed procedure can be applied if the principal residual stress directions are known and the strain gauge rosette is aligned with the principal directions. In the elastic case, the orientation of the rosette does not affect the measurement, as the measured relaxed strain of a strain gauge has a typical tensorial dependency on the orientation angle. The relaxed strain, as a function of the orien-

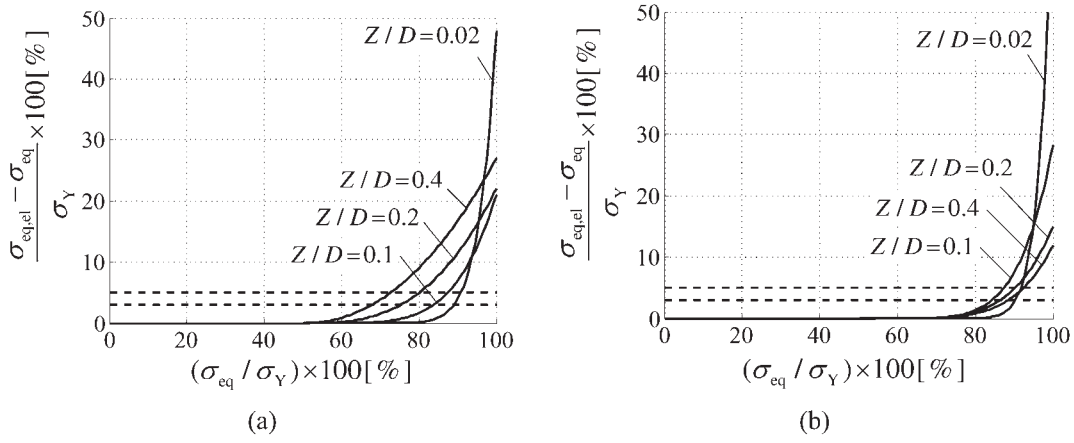

Fig. 14 Proposed procedure effectiveness: (a) equibiaxial residual stress state $\Omega = 1$, (b) pure shear residual stress state $\Omega = -1$

tation angle, only contains a constant and a second-order harmonic term: $\varepsilon(\theta)=\varepsilon'_0+\varepsilon'_1\cos[2(\theta+\phi)]$. As a consequence, in the elastic regime, the entire function can be completely deduced by means of measurements at three angles to find the relaxed strain in the principal directions. Unfortunately, when the plasticity effect plays a part, the total (elastic plus plastic) strain becomes a more complex function of the grid direction angle. This function can be expressed by a typical Fourier expansion including a constant term ε'_0 and a series of harmonics of the type $\varepsilon'_n\cos[2n(\theta+\phi)]$ with $(n=1,2,3\ldots)$. It can be observed that the intensities of higher terms vanish and the following expression is accurate enough: $\varepsilon(\theta)\approx\varepsilon'_0+\varepsilon'_1\cos[2(\theta+\phi)]+\varepsilon'_2\cos[4(\theta+\phi)]$, at least for $f\leqslant 0.9$, while for higher f, the terms $\varepsilon'_3,\varepsilon'_4,\varepsilon'_5$ can also be significant. Assuming that $f\leqslant 0.9$ and unknown principal directions, the number of independent measured strains required is four, being the four unknowns: $\varepsilon'_0,\varepsilon'_1,\varepsilon'_2,\phi$. A rosette carrying four grids with specific angles is required [**17**], or even better, a rosette with more than four grids. The relaxed strain along the principal direction can then be easily evaluated: $\varepsilon_{x(y)}=\varepsilon'_0\pm\varepsilon'_1+\varepsilon'_2$ (ε_x has to be the higher in absolute value). However, in several situations the directions of the principal residual stresses can be deduced by the symmetry of the geometry or by the process which induced the residual stress. For instance, the residual stress produced by shot-peening has to be equibiaxial and every direction is principal, so there is no possibility of misaligning the rosette gauge grids (in this case only one grid would be required). Another example is rolling metalworking; the rolling direction and the orthogonal direction are obviously principal for the residual stress state.

Potentially, the optical methods are more suitable than the rosette method to determine the residual stress in the case of a significant plasticity effect, because the whole strain field could be completely deduced, so the residual stress principal direction would follow.

The proposed procedure also requires that the material yield stress σ_Y is known. It is worth noting that many mechanical processes produce large local plastic strains, such as the shot-peening surface treatment, and then they induce material work-hardening which increases the local yield stress, so the knowledge of the effective yield stress could be rather inaccurate.

The hole geometry does not allow very large plastic strain. Only the first part of the stress–strain curve beyond the yield point is significant in this analysis. For some materials, in this part of the curve the bilinear model may not be simple enough to be adapted as the curve slope can be continuously changing. The strain-hardening ratio should be found by averaging the stress–strain curve up to the maximum strain that the material experiences during the hole drilling and a high R–ratio may be a better choice as compared to a low R–ratio that could be deduced by the whole stress–strain curve of the material. However, this uncertainty is not critical, since the correction function parameters are not very sensitive to the strain-hardening ratio R; see Figs 10(a) and 10(b), so a more complicated material model, which requires many parameters, is not recommended. The correction procedure defined for multiple depths partially faces the complex problem of analysing the high residual stress with a gradient along the depth. A preliminary residual stress evaluation can be produced by adopting the elastic hypotheses in order to find an approximated residual stress distribution. After this, it is common to find the highest level near the surface. In these conditions, the plastic correction might be limited to the smallest depth, while the final part of the residual stress distribution could be approximated as the elastic solution preliminarily found. Otherwise, the correction procedure could be applied for any of the hole depths assuming uniform stress, so deducing approximate information about the depth residual stress distribution. However, for a residual stress evaluation, aimed, for instance, at a fatigue strength assessment, only the residual stress near the surface is of interest, so the procedure can be conveniently used even though the residual stress is not uniform.

6 CONCLUSIONS

A procedure to correct the measurement of high residual stresses, with the blind hole drilling method, has been proposed by taking into account the plasticity effect. All the typical parameters were considered: the rosette type and dimensions, the hole diameter and depth, the material properties, and the stress biaxiality ratios. By means of an extensive FE analysis, an accurate database was obtained in which the effective residual stress loading was related to residual stress deduced by interpreting the relaxed strain assuming the material as elastic. The proposed correcting procedure was derived from a proper elaboration of the FE solutions database. The main results are summarized in the following.

1. The loading-after-hole approach, instead of the correct but more time-consuming hole-after-residual stress approach, introduces a difference not exceeding 3 per cent of the predicted residual stress, so this can be neglected since similar errors are also due to the material yield stress uncertainty, errors in the measurement, procedure fit function approximations, and the uniform stress assumption.
2. The analysis shows that, for deep holes ($Z/D = 0.4$), the error of the elastic solution is less than 3–5 per cent, for residual stresses up to 70 per cent of the material yield stress, and a similar error bound is achieved for residual stresses up to 80–90 per cent of the material yield stress, for shallower holes ($Z/D \leqslant 0.2$). The stress correction procedure described here is useful to reduce stress evaluation errors in cases where the residual stresses are larger than these limits.
3. When residual stresses close to the yield stress are to be measured, a shallow hole is preferred; indeed, this allows the elastic solution to be used without correction or requiring the minimum amount of correction by the method proposed here.
4. Although based on the assumption of uniform stress, the possibility of applying the proposed procedure at different depths can give indications about the as yet unsolved problem of high residual stress with depth gradient.

ACKNOWLEDGEMENTS

The authors are grateful to Eng. Andrea Rossi for his valuable contribution in preparing the models and elaborating the FE results. The SINT Technology Company is also acknowledged for financial and technical support and useful discussions.

REFERENCES

1 *Standard Test Method for Determining Residual Stresses by the Hole-Drilling Strain-Gage Method*, 2008 ASTM E837-08.

2 **Steinzig, M.** and **Ponslet, E.** Residual stress measurement using the hole drilling method and laser speckle interferometry: Part I. *Expl Techqs*, 2003, **27**(3), 43–46.

3 **Ya, M., Dai, F., Xie, H.,** and **Lü, J.** Measurement of non-uniform residual stresses by combined Moiré interferometry and hole-drilling method: Theory, experimental method and applications. *Acta Mech. Sin.*, 2003, **19**(6), 567–574.

4 **Ya, M., Dai, F. L., Xie, H. M.,** and **Lu, J.** Measurement of non-uniform residual stresses by combined Moire interferometry and hole-drilling method: Theory, experimental method and applications. *Acta. Mech. Sin.*, 2003, **19**(6), 567–574.

5 **Ya, M., Marquette, P., Belahcene, F.,** and **Lu, J.** Residual stresses in laser welded aluminium plate by use of ultrasonic and optical methods. *Mater. Sci. Engng A*, 2004, **382**(1–2), 257–264.

6 **Grant, P. V., Lord, P. D.,** and **Whitehead, P. S.** *The measurement of residual stresses by the incremental hole drilling technique*, National Physical Laboratory, 2002. Measurement good practice guide 53.

7 **Gibmeier, J., Nobre, J. P.,** and **Scholtes, B.** Residual stress determination by the hole drilling method in the case of highly stressed surface layers. *Mater. Sci. Res. Int.*, 2004, **10**(1), 21–25.

8 **Gibmeier, J., Kornmeier, M.,** and **Scholtes, B.** Plastic deformation during application of the hole-drilling method. In ECRS 5: Proceedings of the Fifth European Conference on *Residual Stresses*, Materials Science Forum, 2000, **347**(3), 131–136.

9 **Valentini, E., Beghini, M., Bertini, L., Santus, C.,** and **Benedetti, M.** Procedure to perform a validated incremental hole drilling measurement, application to shot peening residual stresses. *Strain*, 2009. In press.

10 **Nobre, J. P., Dias, A. M., Gibmeier, J.,** and **Kornmeier, M.** Local stress-ratio criterion for incremental hole–drilling measurements of shot–peening stresses. *J. Engng Mater. Technol.*, 2006, **128**(2), 193–201.

11 **Nobre, J. P., Loureiro, A., Batista, A. C.,** and **Dias, A. M.** Evaluation of welding residual stresses using the incremental hole-drilling technique. In Advanced Materials Forum III, Parts 1 and 2, Materials Science Forum, 2006, vols 514–516, pp. 768–773.

12 **Moharami, R.** and **Sattari-Far, I.** Experimental and numerical study of measuring high welding residual stresses by using the blind-hole-drilling technique. *J. Strain Analysis*, 2008, **43**(3), 141–148. DOI: 10.1243/03093247JSA378.

13 **Fratini, L.** and **Zuccarello, B.** An analysis of through-thickness residual stresses in aluminium FSW butt joints. *Int. J. Mach. Tools Mf.*, 2006, **46**(6), 611–619.

14 **Timoshenko, S. P.** and **Goodier, J. N.** *Theory of elasticity,* 3rd edition, 1970 (McGraw-Hill, New York).

15 **Beghini, M., Bertini, L.,** and **Raffaelli, P.** An account of plasticity in the hole-drilling method of residual stress measurement. *J. Strain Analysis*, 1995, **30**(3), 227–233. DOI: 10.1243/03093247V303227.

16 **Beghini, M., Bertini, L.,** and **Raffaelli, P.** Numerical analysis of plasticity effects in the hole-drilling residual stress measurement. *J. Test. Eval.*, 1994, **22**(6), 522–529.

17 **Beghini, M.** and **Bertini, L.** Recent advances in the hole drilling method for residual stress measurement. *J. Mater. Engng Perform.*, 1998, **7**(2), 163–172.

18 Vishay. Strain-Gages Datasheets, available from http://www.vishay.com/.

19 HBM. Strain-Gages Datasheets, available from http://www.hbm.com/.

20 **Beghini, M., Bertini, L.,** and **Mori, L. F.** Evaluating non-uniform residual stress by the hole-drilling method with concentric and eccentric holes. Part I: Definition and validation of the influence functions. *Strain*, 2009. In press.

21 **Schajer, G. S.** Application of finite element calculations to residual stress measurements. *J. Engng Mater. Technol.*, 1981, **103**(2), 157–163.

APPENDIX 1

Notation

a, b	elastic calibration coefficients
d_p	path dependency
D	diameter of the gauge circle
D_0	diameter of the drilled hole
e_v	error defined to validate the model
E, ν	material elastic constants: Young's modulus and Poisson's ratio
E_T	tangent modulus in the elastic–plastic regime
f	plasticity factor
$\hat{f}$	procedure estimated plasticity factor
f_{el}	plasticity factor, calculated from the elastically calculated residual stresses
G_L	gauge length
G_W	gauge width
H	specimen thickness
$R = E_T/E$	strain hardening ratio
w_i, m_i	approximation fit coefficients to find the parameters W, m respectively
W, μ	parameters of the approximation fit function $f - f_{el}$
Z	hole depth
Z_1, Z_2, Z_3, Z_4	hole depths used in the application example
$\delta = D_0/D$	ratio between gauge circle and drilled hole diameters
ε_x, ε_y	relaxed strains along the principal residual stress directions
ε_1, ε_2, ε_3	relaxed strains along the grid directions
$\varepsilon'_0, \varepsilon'_1, \varepsilon'_2, \ldots$	relaxed strain function harmonic intensities (even order terms only)
ε_1^{pl}	first principal plastic strain
σ_{eq}	equivalent residual stress (von Mises)
$\hat{\sigma}_{eq}$	procedure estimated equivalent residual stress
$\sigma_{eq,i}$	equivalent residual stress at the onset of yielding
$\sigma_{eq,el}$	equivalent residual stress, considering the material as elastic
$\sigma_{x,el}$, $\sigma_{y,el}$	residual principal stresses, considering the material as elastic
$\hat{\sigma}_x$, $\hat{\sigma}_x$	estimated principal residual stress components
σ_x, σ_y	residual principal stresses
σ_Y	material (initial) yield stress
Ω_{el}	stress biaxiality ratio, considering the material as elastic
$\Omega = \sigma_y/\sigma_x$	residual stress biaxiality ratio

APPENDIX 2

Tabular results of coefficients

Table 3 Elastic calibration coefficients, different rosettes, and hole depths

		$Z/D = 0.02$ $D_0/D = 0.3$	$D_0/D = 0.35$	$D_0/D = 0.4$	$D_0/D = 0.45$	$D_0/D = 0.5$
ASTM A	a	0.00858	0.01186	0.01596	0.02116	0.02797
	b	0.01604	0.02180	0.02868	0.03699	0.04729
ASTM B	a	0.00909	0.01256	0.01696	0.02250	0.02984
	b	0.01776	0.02407	0.03164	0.04066	0.05189
HBM 1	a	0.00875	0.01209	0.01629	0.02155	0.02836
	b	0.01696	0.02302	0.03026	0.03887	0.04935
HBM 2	a	0.00922	0.01272	0.01724	0.02274	0.03010
	b	0.01863	0.02517	0.03317	0.04234	0.05376
HBM 3	a	0.00920	0.01270	0.01722	0.02271	0.03005
	b	0.01858	0.02511	0.03309	0.04225	0.05363

		$Z/D = 0.1$ $D_0/D = 0.3$	$D_0/D = 0.35$	$D_0/D = 0.4$	$D_0/D = 0.45$	$D_0/D = 0.5$
ASTM A	a	0.0589	0.0806	0.1069	0.1389	0.1779
	b	0.1147	0.1536	0.1985	0.2509	0.3116

Table 3 (continued)

		$Z/D = 0.1$ $D_0/D = 0.3$	$D_0/D = 0.35$	$D_0/D = 0.4$	$D_0/D = 0.45$	$D_0/D = 0.5$
ASTM B	*a*	0.0622	0.0852	0.1132	0.1470	0.1886
	b	0.1274	0.1702	0.2199	0.2767	0.3426
HBM 1	*a*	0.0601	0.0824	0.1095	0.1421	0.1817
	b	0.1220	0.1632	0.2110	0.2661	0.3291
HBM 2	*a*	0.0632	0.0865	0.1155	0.1495	0.1916
	b	0.1344	0.1791	0.2319	0.2908	0.3588
HBM 3	*a*	0.0631	0.0864	0.1153	0.1493	0.1913
	b	0.1340	0.1787	0.2314	0.2902	0.3580
		$Z/D = 0.2$ $D_0/D = 0.3$	$D_0/D = 0.35$	$D_0/D = 0.4$	$D_0/D = 0.45$	$D_0/D = 0.5$
ASTM A	*a*	0.1011	0.1368	0.1773	0.2232	0.2739
	b	0.2188	0.2888	0.3643	0.4453	0.5290
ASTM B	*a*	0.1062	0.1437	0.1864	0.2343	0.2874
	b	0.2433	0.3202	0.4029	0.4903	0.5793
HBM 1	*a*	0.1037	0.1405	0.1824	0.2299	0.2819
	b	0.2346	0.3095	0.3905	0.4772	0.5650
HBM 2	*a*	0.1085	0.1467	0.1910	0.2402	0.2943
	b	0.2585	0.3397	0.4283	0.5206	0.6131
HBM 3	*a*	0.1084	0.1466	0.1907	0.2399	0.2939
	b	0.2579	0.3388	0.4273	0.5195	0.6118
		$Z/D = 0.4$ $D_0/D = 0.3$	$D_0/D = 0.35$	$D_0/D = 0.4$	$D_0/D = 0.45$	$D_0/D = 0.5$
ASTM A	*a*	0.1108	0.1487	0.1907	0.2370	0.2873
	b	0.2838	0.3706	0.4598	0.5505	0.6385
ASTM B	*a*	0.1160	0.1558	0.1998	0.2483	0.3010
	b	0.3172	0.4130	0.5109	0.6090	0.7026
HBM 1	*a*	0.1141	0.1531	0.1966	0.2445	0.2959
	b	0.3076	0.4010	0.4974	0.5951	0.6875
HBM 2	*a*	0.1189	0.1595	0.2051	0.2548	0.3085
	b	0.3401	0.4419	0.5472	0.6516	0.7485
HBM 3	*a*	0.1188	0.1593	0.2049	0.2546	0.3081
	b	0.3392	0.4408	0.5459	0.6500	0.7468

Table 4 Fit function coefficients: w_i, $m_i (i = 1, \ldots, 12)$, different rosettes, strain hardening ratios, and hole depths

$Z/D = 0.02$ $R = 0.01$	ASTM A	ASTM B	HBM 1	HBM 2	HBM 3		ASTM A	ASTM B	HBM 1	HBM 2	HBM 3
w_1	−4.191	−5.064	−4.657	−5.475	−5.451	m_1	−35.36	−40.23	−38.01	−41.69	−41.46
w_2	−0.806	−0.712	−0.711	−0.645	−0.646	m_2	27.77	28.58	28.08	29.73	29.79
w_3	4.086	5.850	5.167	6.760	6.712	m_3	51.39	53.32	51.82	49.70	49.79
w_4	9.981	8.485	9.383	8.038	8.101	m_4	−19.62	−19.11	−17.23	−14.07	−14.84
w_5	3.455	4.152	3.886	4.555	4.535	m_5	42.31	48.58	46.54	52.28	52.01
w_6	0.872	0.701	0.720	0.554	0.558	m_6	−13.63	−13.87	−13.79	−14.59	−14.67
w_7	−2.346	−3.855	−3.374	−4.754	−4.713	m_7	−55.52	−61.24	−59.55	−62.96	−62.85
w_8	−11.963	−10.454	−11.265	−9.883	−9.943	m_8	3.10	4.60	2.90	2.60	3.17
w_9	−0.525	−0.647	−0.609	−0.725	−0.722	m_9	−11.18	−12.43	−12.11	−13.29	−13.23
w_{10}	−0.203	−0.143	−0.153	−0.093	−0.095	m_{10}	−1.81	−1.59	−1.65	−1.35	−1.34
w_{11}	−0.175	0.135	0.048	0.326	0.318	m_{11}	12.06	13.46	13.18	14.19	14.15
w_{12}	4.390	3.993	4.198	3.836	3.850	m_{12}	17.86	16.93	17.49	16.92	16.83
$Z/D = 0.02$ $R = 0.1$	ASTM A	ASTM B	HBM 1	HBM 2	HBM 3		ASTM A	ASTM B	HBM 1	HBM 2	HBM 3
w_1	−2.949	−3.650	−3.366	−4.011	−3.990	m_1	−31.83	−35.63	−34.29	−37.08	−36.69
w_2	−0.760	−0.705	−0.713	−0.663	−0.664	m_2	26.79	26.87	26.37	27.38	27.44
w_3	2.838	4.275	3.760	5.043	5.004	m_3	48.54	49.43	48.85	46.24	46.19
w_4	9.695	8.415	9.226	8.054	8.112	m_4	−16.90	−15.73	−13.94	−10.45	−11.25
w_5	2.363	2.931	2.748	3.276	3.259	m_5	39.47	44.80	43.46	48.30	47.91
w_6	0.806	0.679	0.704	0.571	0.574	m_6	−12.98	−12.69	−12.59	−12.91	−12.98

Table 4 (continued)

$Z/D = 0.02$ $R = 0.1$

	ASTM A	ASTM B	HBM 1	HBM 2	HBM 3		ASTM A	ASTM B	HBM 1	HBM 2	HBM 3
w_7	−1.398	−2.646	−2.282	−3.402	−3.368	m_7	−53.71	−58.33	−57.43	−59.99	−59.79
w_8	−11.475	−10.159	−10.901	−9.687	−9.742	m_8	−0.01	0.87	−0.76	−1.50	−0.91
w_9	−0.293	−0.396	−0.370	−0.463	−0.460	m_9	−10.83	−11.90	−11.72	−12.72	−12.64
w_{10}	−0.188	−0.138	−0.149	−0.098	−0.099	m_{10}	−2.04	−1.90	−1.98	−1.75	−1.74
w_{11}	−0.328	−0.063	−0.131	0.100	0.093	m_{11}	12.06	13.24	13.11	13.93	13.88
w_{12}	4.110	3.753	3.944	3.617	3.631	m_{12}	19.02	18.17	18.75	18.24	18.14

$Z/D = 0.02$ $R = 0.25$

	ASTM A	ASTM B	HBM 1	HBM 2	HBM 3		ASTM A	ASTM B	HBM 1	HBM 2	HBM 3
w_1	−1.609	−2.125	−1.932	−2.403	−2.387	m_1	−27.32	−29.77	−29.20	−30.90	−30.46
w_2	−0.651	−0.607	−0.620	−0.568	−0.567	m_2	26.45	25.49	25.40	25.48	25.41
w_3	1.434	2.512	2.135	3.098	3.067	m_3	44.78	44.48	44.71	41.31	41.05
w_4	9.319	8.249	8.946	7.954	8.003	m_4	−12.18	−10.36	−8.85	−4.74	−5.89
w_5	1.211	1.644	1.514	1.910	1.897	m_5	36.34	40.55	39.77	43.62	43.15
w_6	0.687	0.585	0.610	0.500	0.501	m_6	−12.77	−11.66	−11.89	−11.48	−11.44
w_7	−0.381	−1.348	−1.070	−1.933	−1.906	m_7	−52.00	−55.45	−55.20	−56.72	−56.34
w_8	−10.836	−9.713	−10.365	−9.326	−9.373	m_8	−5.92	−5.61	−7.04	−8.45	−7.57
w_9	−0.070	−0.155	−0.134	−0.209	−0.207	m_9	−10.68	−11.58	−11.49	−12.31	−12.21
w_{10}	−0.167	−0.125	−0.134	−0.092	−0.093	m_{10}	−2.34	−2.34	−2.35	−2.25	−2.27
w_{11}	−0.451	−0.234	−0.290	−0.101	−0.107	m_{11}	12.44	13.42	13.41	14.03	13.95
w_{12}	3.742	3.427	3.599	3.311	3.323	m_{12}	21.46	20.66	21.23	20.80	20.64

$Z/D = 0.1$ $R = 0.01$

	ASTM A	ASTM B	HBM 1	HBM 2	HBM 3		ASTM A	ASTM B	HBM 1	HBM 2	HBM 3
w_1	−4.322	−5.171	−4.957	−5.773	−5.755	m_1	5.73	1.23	4.02	−0.33	−0.23
w_2	−1.396	−1.294	−1.304	−1.005	−1.014	m_2	15.08	17.79	16.30	20.62	20.47
w_3	3.464	5.118	4.658	6.121	6.090	m_3	−11.55	−3.29	−7.58	−0.38	−0.55
w_4	2.804	1.894	2.250	1.273	1.302	m_4	−3.59	−8.92	−7.17	−13.47	−13.28
w_5	4.010	4.642	4.528	5.134	5.120	m_5	−7.93	−4.64	−6.31	−3.54	−3.60
w_6	1.765	1.612	1.648	1.295	1.306	m_6	−8.40	−10.28	−9.34	−12.58	−12.47
w_7	−3.079	−4.462	−4.124	−5.340	−5.313	m_7	16.34	9.47	12.40	6.90	7.01
w_8	−4.039	−3.130	−3.449	−2.463	−2.493	m_8	1.37	6.31	4.79	10.45	10.29
w_9	−0.872	−0.947	−0.946	−1.013	−1.011	m_9	1.83	1.16	1.43	0.91	0.92
w_{10}	−0.487	−0.433	−0.451	−0.349	−0.352	m_{10}	0.09	0.41	0.25	0.87	0.85
w_{11}	0.563	0.804	0.752	0.952	0.948	m_{11}	−4.74	−3.24	−3.78	−2.63	−2.65
w_{12}	1.659	1.431	1.514	1.271	1.278	m_{12}	6.39	5.27	5.62	4.37	4.40

$Z/D = 0.1$ $R = 0.1$

	ASTM A	ASTM B	HBM 1	HBM 2	HBM 3		ASTM A	ASTM B	HBM 1	HBM 2	HBM 3
w_1	−2.006	−2.664	−2.447	−3.123	−3.107	m_1	−2.36	−5.38	−2.94	−6.17	−6.09
w_2	−1.271	−1.253	−1.262	−1.069	−1.079	m_2	9.61	11.71	10.42	14.40	14.22
w_3	1.541	2.826	2.425	3.600	3.573	m_3	−2.94	3.57	−0.21	5.65	5.50
w_4	2.446	1.767	2.056	1.324	1.349	m_4	0.90	−3.91	−2.30	−8.23	−8.02
w_5	1.967	2.481	2.343	2.868	2.855	m_5	−1.10	1.08	−0.39	1.62	1.58
w_6	1.467	1.394	1.425	1.191	1.201	m_6	−4.33	−5.75	−4.94	−7.84	−7.71
w_7	−1.400	−2.500	−2.193	−3.188	−3.165	m_7	9.20	3.69	6.28	1.73	1.84
w_8	−3.409	−2.724	−2.981	−2.248	−2.272	m_8	−2.23	2.23	0.83	6.04	5.87
w_9	−0.417	−0.487	−0.473	−0.542	−0.541	m_9	0.59	0.09	0.35	−0.08	−0.07
w_{10}	−0.381	−0.345	−0.360	−0.288	−0.291	m_{10}	−0.67	−0.41	−0.56	0.00	−0.02
w_{11}	0.201	0.402	0.349	0.522	0.518	m_{11}	−3.41	−2.13	−2.63	−1.62	−1.65
w_{12}	1.374	1.197	1.265	1.081	1.087	m_{12}	6.93	5.89	6.22	5.07	5.11

$Z/D = 0.1$ $R = 0.25$

	ASTM A	ASTM B	HBM 1	HBM 2	HBM 3		ASTM A	ASTM B	HBM 1	HBM 2	HBM 3
w_1	−1.541	−1.984	−1.820	−2.291	−2.278	m_1	−1.46	−3.94	−1.55	−4.16	−4.09
w_2	−0.903	−0.942	−0.935	−0.861	−0.866	m_2	7.60	9.26	8.13	11.52	11.37
w_3	1.190	2.082	1.791	2.617	2.595	m_3	−4.05	1.68	−1.85	3.24	3.10
w_4	1.891	1.435	1.639	1.162	1.179	m_4	3.28	−1.16	0.33	−5.05	−4.86
w_5	1.436	1.795	1.684	2.059	2.049	m_5	−2.10	−0.35	−1.83	−0.27	−0.31
w_6	1.012	1.002	1.014	0.903	0.908	m_6	−3.06	−4.17	−3.45	−5.88	−5.77
w_7	−1.008	−1.787	−1.559	−2.268	−2.249	m_7	10.47	5.64	8.07	4.15	4.25
w_8	−2.595	−2.128	−2.311	−1.830	−1.846	m_8	−4.19	−0.06	−1.39	3.32	3.16
w_9	−0.274	−0.328	−0.314	−0.368	−0.366	m_9	0.97	0.54	0.80	0.44	0.45
w_{10}	−0.255	−0.236	−0.245	−0.204	−0.206	m_{10}	−0.88	−0.67	−0.80	−0.33	−0.35
w_{11}	0.107	0.256	0.214	0.342	0.339	m_{11}	−3.85	−2.69	−3.17	−2.26	−2.28
w_{12}	1.035	0.911	0.960	0.835	0.839	m_{12}	7.23	6.25	6.57	5.51	5.55

Table 4 (continued)

$Z/D = 0.2$ $R = 0.01$											
	ASTM A	ASTM B	HBM 1	HBM 2	HBM 3		ASTM A	ASTM B	HBM 1	HBM 2	HBM 3
w_1	−3.758	−4.157	−4.224	−4.676	−4.659	m_1	−30.41	−34.62	−35.17	−41.37	−41.15
w_2	−0.022	−0.007	−0.129	−0.024	−0.032	m_2	26.25	25.88	25.07	24.06	24.07
w_3	3.215	4.350	4.084	5.233	5.199	m_3	11.41	20.15	18.25	30.99	30.57
w_4	3.770	3.136	3.406	2.691	2.715	m_4	4.03	0.45	2.80	−3.05	−2.83
w_5	3.523	3.753	3.858	4.098	4.087	m_5	15.86	17.31	18.35	20.52	20.44
w_6	0.502	0.459	0.555	0.406	0.415	m_6	−18.71	−18.24	−17.85	−17.07	−17.08
w_7	−3.424	−4.393	−4.201	−5.123	−5.097	m_7	−0.08	−6.11	−4.98	−12.97	−12.71
w_8	−4.583	−3.867	−4.135	−3.352	−3.377	m_8	−3.24	0.73	−1.31	4.24	4.05
w_9	−0.862	−0.852	−0.888	−0.872	−0.872	m_9	−1.73	−1.98	−2.18	−2.45	−2.44
w_{10}	−0.180	−0.150	−0.174	−0.116	−0.118	m_{10}	2.99	2.80	2.76	2.58	2.58
w_{11}	0.978	1.142	1.116	1.254	1.250	m_{11}	−2.61	−1.22	−1.48	0.08	0.04
w_{12}	1.579	1.379	1.452	1.242	1.248	m_{12}	5.06	4.08	4.51	3.27	3.31

$Z/D = 0.2$ $R = 0.1$											
	ASTM A	ASTM B	HBM 1	HBM 2	HBM 3		ASTM A	ASTM B	HBM 1	HBM 2	HBM 3
w_1	−2.317	−2.682	−2.743	−3.073	−3.062	m_1	−5.92	−9.62	−10.71	−14.86	−14.71
w_2	−0.027	−0.112	−0.197	−0.177	−0.184	m_2	16.88	17.16	16.18	16.33	16.28
w_3	1.752	2.747	2.525	3.420	3.396	m_3	−9.21	−0.59	−2.14	8.38	8.05
w_4	2.839	2.371	2.575	2.052	2.071	m_4	7.39	2.80	5.30	−1.23	−0.98
w_5	2.202	2.470	2.545	2.757	2.750	m_5	−3.11	−1.48	−0.20	1.06	1.01
w_6	0.339	0.385	0.452	0.395	0.402	m_6	−11.79	−11.71	−11.18	−11.16	−11.12
w_7	−2.050	−2.939	−2.764	−3.526	−3.506	m_7	16.56	10.04	11.06	4.09	4.30
w_8	−3.511	−2.980	−3.184	−2.613	−2.633	m_8	−6.60	−1.98	−4.11	1.80	1.59
w_9	−0.539	−0.557	−0.582	−0.584	−0.584	m_9	2.00	1.64	1.42	1.22	1.23
w_{10}	−0.112	−0.102	−0.120	−0.086	−0.088	m_{10}	1.68	1.57	1.50	1.45	1.45
w_{11}	0.636	0.800	0.771	0.898	0.895	m_{11}	−5.95	−4.39	−4.65	−3.18	−3.22
w_{12}	1.232	1.079	1.135	0.979	0.984	m_{12}	5.72	4.61	5.06	3.76	3.80

$Z/D = 0.2$ $R = 0.25$											
	ASTM A	ASTM B	HBM 1	HBM 2	HBM 3		ASTM A	ASTM B	HBM 1	HBM 2	HBM 3
w_1	−1.101	−1.418	−1.428	−1.726	−1.717	m_1	−8.58	−13.09	−13.92	−19.11	−18.94
w_2	−0.125	−0.198	−0.271	−0.272	−0.276	m_2	14.80	14.50	13.62	13.36	13.35
w_3	0.770	1.552	1.359	2.059	2.041	m_3	−4.55	4.70	3.16	14.04	13.71
w_4	2.173	1.836	1.982	1.627	1.639	m_4	8.01	4.15	6.25	0.97	1.17
w_5	1.108	1.360	1.382	1.599	1.593	m_5	0.10	2.45	3.50	5.73	5.67
w_6	0.283	0.328	0.388	0.366	0.369	m_6	−10.53	−10.02	−9.52	−9.17	−9.16
w_7	−1.059	−1.767	−1.609	−2.217	−2.201	m_7	12.03	4.99	6.02	−1.34	−1.12
w_8	−2.632	−2.257	−2.403	−2.020	−2.033	m_8	−7.34	−3.39	−5.21	−0.36	−0.54
w_9	−0.274	−0.304	−0.314	−0.334	−0.334	m_9	1.29	0.79	0.61	0.22	0.23
w_{10}	−0.071	−0.066	−0.082	−0.061	−0.062	m_{10}	1.45	1.27	1.19	1.09	1.09
w_{11}	0.359	0.497	0.469	0.577	0.575	m_{11}	−4.99	−3.33	−3.59	−2.05	−2.09
w_{12}	0.908	0.800	0.840	0.734	0.737	m_{12}	5.81	4.83	5.23	4.12	4.16

$Z/D = 0.4$ $R = 0.01$											
	ASTM A	ASTM B	HBM 1	HBM 2	HBM 3		ASTM A	ASTM B	HBM 1	HBM 2	HBM 3
w_1	−1.579	−1.604	−1.750	−1.567	−1.568	m_1	6.11	6.91	6.52	9.38	9.30
w_2	1.636	1.847	1.753	1.704	1.706	m_2	16.56	22.63	22.18	20.11	20.30
w_3	0.348	0.783	0.690	1.246	1.223	m_3	−20.14	−25.83	−26.06	−23.21	−23.49
w_4	4.662	4.017	4.355	3.619	3.644	m_4	11.99	10.26	11.97	7.10	7.31
w_5	1.950	1.924	2.020	1.786	1.788	m_5	−12.47	−12.63	−12.58	−15.59	−15.51
w_6	−0.569	−0.733	−0.706	−0.677	−0.678	m_6	−8.93	−14.37	−14.04	−12.89	−13.02
w_7	−1.383	−1.904	−1.784	−2.324	−2.303	m_7	21.64	25.41	25.84	24.22	24.41
w_8	−5.469	−4.673	−4.997	−4.162	−4.188	m_8	−11.04	−8.47	−9.97	−5.37	−5.56
w_9	−0.841	−0.778	−0.803	−0.695	−0.697	m_9	2.93	2.64	2.74	3.15	3.14
w_{10}	−0.042	0.013	0.008	0.032	0.031	m_{10}	1.43	2.42	2.38	2.10	2.12
w_{11}	0.965	1.060	1.039	1.119	1.116	m_{11}	−5.88	−6.02	−6.26	−5.57	−5.61
w_{12}	1.846	1.602	1.686	1.445	1.452	m_{12}	5.81	5.07	5.40	4.35	4.39

$Z/D = 0.4$ $R = 0.1$											
	ASTM A	ASTM B	HBM 1	HBM 2	HBM 3		ASTM A	ASTM B	HBM 1	HBM 2	HBM 3
w_1	0.494	0.357	0.196	0.295	0.297	m_1	13.01	12.18	11.60	14.90	14.84
w_2	1.539	1.592	1.521	1.396	1.398	m_2	17.08	22.05	22.02	18.90	19.07
w_3	−1.437	−0.836	−0.929	−0.354	−0.375	m_3	−26.95	−28.67	−29.66	−25.81	−26.10
w_4	3.280	2.759	3.033	2.474	2.494	m_4	10.26	7.39	9.39	4.56	4.77
w_5	−0.015	0.090	0.190	0.067	0.067	m_5	−16.43	−15.55	−15.26	−18.63	−18.56

Table 4 (continued)

$Z/D = 0.4$ $R = 0.1$	ASTM A	ASTM B	HBM 1	HBM 2	HBM 3		ASTM A	ASTM B	HBM 1	HBM 2	HBM 3
w_6	−0.746	−0.773	−0.756	−0.654	−0.655	m_6	−10.54	−14.76	−14.83	−12.58	−12.70
w_7	0.442	−0.202	−0.084	−0.637	−0.619	m_7	26.63	27.29	28.27	25.68	25.88
w_8	−3.933	−3.312	−3.572	−2.946	−2.966	m_8	−9.61	−6.31	−8.00	−3.50	−3.68
w_9	−0.279	−0.264	−0.285	−0.220	−0.222	m_9	3.69	3.27	3.31	3.83	3.81
w_{10}	0.053	0.076	0.073	0.076	0.075	m_{10}	1.76	2.48	2.52	2.01	2.03
w_{11}	0.401	0.530	0.507	0.602	0.599	m_{11}	−6.78	−6.38	−6.70	−5.85	−5.89
w_{12}	1.361	1.173	1.239	1.058	1.064	m_{12}	5.37	4.51	4.87	3.84	3.88
$Z/D = 0.4$ $R = 0.25$	ASTM A	ASTM B	HBM 1	HBM 2	HBM 3		ASTM A	ASTM B	HBM 1	HBM 2	HBM 3
w_1	0.773	0.575	0.432	0.411	0.413	m_1	8.74	6.15	5.40	6.75	6.73
w_2	1.015	1.022	0.954	0.841	0.843	m_2	14.63	19.02	18.99	15.93	16.09
w_3	−1.499	−0.927	−0.996	−0.462	−0.478	m_3	−20.56	−19.96	−20.98	−15.58	−15.88
w_4	2.323	1.961	2.161	1.782	1.795	m_4	10.59	8.00	9.88	5.81	5.99
w_5	−0.470	−0.292	−0.206	−0.200	−0.201	m_5	−13.21	−10.95	−10.55	−12.25	−12.20
w_6	−0.517	−0.506	−0.482	−0.382	−0.384	m_6	−8.76	−12.47	−12.55	−10.29	−10.41
w_7	0.833	0.238	0.330	−0.182	−0.167	m_7	22.23	21.08	22.09	18.11	18.32
w_8	−2.764	−2.338	−2.526	−2.104	−2.118	m_8	−10.38	−7.35	−8.96	−5.04	−5.20
w_9	−0.054	−0.072	−0.087	−0.066	−0.067	m_9	3.31	2.65	2.67	2.86	2.85
w_{10}	0.053	0.063	0.059	0.055	0.055	m_{10}	1.34	1.96	2.01	1.50	1.52
w_{11}	0.131	0.258	0.238	0.336	0.333	m_{11}	−6.19	−5.46	−5.78	−4.66	−4.71
w_{12}	0.953	0.823	0.871	0.747	0.751	m_{12}	5.54	4.72	5.08	4.15	4.18

APPENDIX 3

Newton–Raphson algorithm to find the plasticity factor

In order to solve equation (7) numerically to obtain the actual plasticity factor f when the elastically calculated plasticity factor f_{el} is known, the Newton–Raphson algorithm was found to be efficiently convergent when properly adapted to the problem. In the following, some useful suggestions are provided for the practical solution of this problem. By assuming that the quantities W, μ are known, the following algorithm produces a convergent sequence of approximations of the (actual) plasticity factor f

$$\hat{f}_1 = \min\{1, f_{el}\}$$

$$\hat{f}_{i+1} = \hat{f}_i - \frac{W\hat{f}_i^{\mu} + \hat{f}_i - f_{el}}{\mu W \hat{f}_i^{\mu-1} + 1} \tag{12}$$

It was verified that, with the initial value here suggested, the error $|\hat{f}_i - f|/f$ is always below 1 per cent when $i \geqslant 5$; thus, for practical applications it can be assumed that

$$\hat{f} = \hat{f}_5 \tag{13}$$

A different initial value can require a larger number of iterations to reach a numerical solution $\hat{f}$ having similar precision.